ISSN 1063-7850, Technical Physics Letters, 2020, Vol. 46, No. 7, pp. 687–690. © Pleiades Publishing, Ltd., 2020.
Russian Text © The Author(s), 2020, published in Pis'ma v Zhurnal Tekhnicheskoi Fiziki, 2020, Vol. 46, No. 14, pp. 13–16.

Silicon Nanoparticles Formed via Pulsed Laser Ablation of Porous Silicon in Liquids

A. V. Skobelkina[a]*, F. V. Kashaev[a], A. V. Kolchin[a], D. V. Shuleiko[a], T. P. Kaminskaya[a], D. E. Presnov[a,b,c], L. A. Golovan[a], and P. K. Kashkarov[a,d]

[a] *Faculty of Physics, Moscow State University, Moscow, 119991 Russia*
[b] *Skobeltsyn Research Institute of Nuclear Physics, Moscow State University, Moscow, 119991 Russia*
[c] *Center of Quantum Technologies, Moscow State University, Moscow, 119991 Russia*
[d] *National Research Center "Kurchatov Institute," Moscow, 123182 Russia*
**e-mail: snastya.19996@mail.ru*

Received March 26, 2020; revised March 26, 2020; accepted April 10, 2020

Abstract—Picosecond pulsed laser ablation of meso- and microporous silicon layers in water and ethanol leads to the formation of nanosilicon suspensions with particle diameters below 100 nm. It is established that the use of porous silicon targets allows the laser ablation threshold to be reduced and the nanoparticle concentration increased as compared to the ablation of crystalline silicon.

Keywords: pulsed laser ablation, porous silicon, atomic force microscopy, ablation threshold.

DOI: 10.1134/S1063785020070263

In recent years, much effort has been devoted to the application of silicon nanoparticles (Si-NPs) to solving various biomedical problems [1–3]. This interest in Si-NPs is related to their high biocompatibility, biodegradability, and low toxicity. For effective introduction into biological tissues, particle sizes must be below 100 nm. Existing methods of mechanical of ultrasonic comminution, which are traditionally applied to porous (*por*-Si) and single-crystalline silicon (*c*-Si) cannot meet this requirement [4]. At the same time, the task of obtaining NPs with diameters below 100 nm can be solved by means of pulsed laser ablation in a liquid medium, and the obtained Si-NP suspensions have proved to be chemically pure [3]. However, the yield of reaction product from this process is rather low, which hinders the use of such Si-NPs in view of their low concentration in the suspension. To eliminate this disadvantage, it is possible to form Si-NPs by laser ablation of porous silicon (*por*-Si), a nanocomposite medium comprising silicon nanocrystals separated by nanopores [5], which can be obtained be electrochemical etching of *c*-Si wafers in an appropriate electrolyte. Depending on the properties of the initial *c*-Si wafers and electrolyte, this treatment leads to the formation of a layer of either microporous silicon (micropor-Si) with sizes of both pores and nanocrystals not exceeding 10 nm or mesoporous silicon (mesopor-Si) with sizes of both pores and nanocrystals within 10–50 nm.

A two-stage process involving (i) formation of a porous layer by electrochemical etching of *c*-Si and (ii) subsequent laser ablation of obtained *por*-Si yields Si-NPs that are highly requested in various biomedical applications [6]. These include photoluminescent labels [6], contrast agents in optical coherent tomography [7], and photosensitizers of singlet oxygen in photodynamic therapy [7]. However, the formation of Si-NPs meeting requirements of these applications is only possible provided that the laser radiation parameters are known that allow obtaining Si-NPs with a required structure. One of the main parameters is the laser ablation threshold, that is, the minimum energy density sufficient for effective ablation of the target material and formation of a crater on the *por*-Si target surface. In addition, it is also necessary to determine the dimensions of obtained Si-NPs and their concentration in suspension after termination of the laser ablation process.

In this work, micropor-Si and mesopor-Si layers were prepared from single-crystalline *p*-type silicon wafers with a (100) surface orientation and resistivity of 10–20 and 17–23 Ω cm, respectively, which were subjected to electrochemical etching at 75-mA/cm^2 current density for 30 min in an aqueous hydrofluoric acid–ethanol mixture [8]. The average thicknesses of obtained micropor-Si and micropor-Si layers, as estimated by scanning electron microscopy (SEM) using a Carl Zeiss Supra-40 instrument, amounted to 25 and 80 μm, respectively.

To determine the laser ablation threshold, the initial *c*-Si wafers and final *por*-Si layers were exposed to

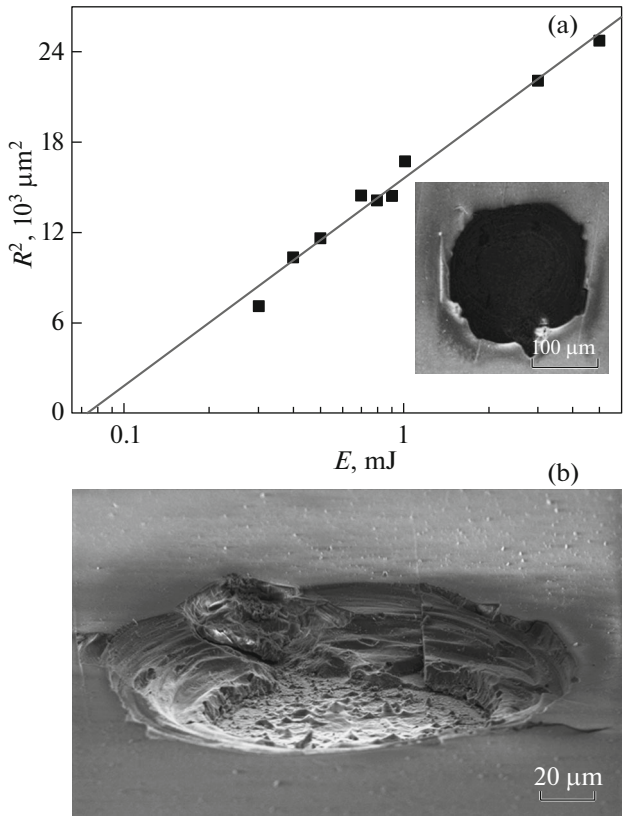

Fig. 1. (a) Experimental plot of R^2 vs. E (points) for single-pulse laser action on micropor-Si layer in air and its linear approximation (straight line), for which $\omega_0^2 = 5986 \pm 316$ μm^2 and $F_{th} = 0.41 \pm 0.02$ J/cm^2; the inset shows SEM image of the crater upon single-pulse laser action on micropor-Si layer in air. (b) SEM image of the ablation crater (viewed at 45°) upon single-pulse laser action on micropor-Si layer in air.

single pulses of EKSPLA 2143A (1064 nm, 30 ps) with energies from 0.3 to 5 mJ. The laser beam was focused by a lens with a 40-mm focal distance onto the sample surface in air or under a 5-mm-thick layer of distilled water or ethanol. After each exposure, the substrate with the sample was shifted by certain distance with the aid of a step-motor drive. The ablation thresholds in all materials were determined by measuring radius R of ablation craters in Olimpus BX41 microscope (Figs. 1a, 1b) and plotting R^2 versus laser pulse energy E (see the typical pattern in Fig. 1a).

For a laser beam with Gaussian field distribution in a single pulse of energy E, square radius R^2 of the ablation crater is a linear function of energy density F, which is related to pulse energy E as

$$R^2 = \omega_0^2 \ln(F/F_{th}), \quad (1)$$

where

$$F = 2E/\pi\omega_0^2, \quad (2)$$

ω_0^2 is the Gaussian beam radius at a $1/e^2$ intensity level, and F_{th} is the threshold energy density. As can be seen from Fig. 1a, the $R^2(E)$ plot is close to linear. Therefore, square radius ω_0^2 can be determined from the plot of $R^2(E)$ by using its linear approximation (Fig. 1a). Then, the laser energy can be converted into energy density and ablation threshold F_{abl} can be found by extrapolating the aforementioned dependence to zero ordinate (R^2) [9, 10]. The dependences of the crater diameter on the ablation energy density in liquid media possess a similar character and exhibit growth with the energy in the entire range studied.

Based on an analysis of the surface morphology, it is possible to draw conclusions concerning the mechanism of laser energy absorption by the target material during single-pulse ablation process. The observed linear decrease in the crater radius with decreasing laser pulse energy suggests that two-photon absorption contributes to this single-pulse ablation process. A decrease in the laser energy is accompanied by growing contribution of multiphoton processes that lead to reduction in area of the ablation spot [11]. It should be noted that the linear character of the $R^2(E)$ plot also suggests that a sufficiently high ablation energy can result in the ejection of large pieces of target material. Calculated values of the threshold ablation energy in water and ethanol are listed in Table 1, where a decrease in the ablation threshold for *por*-Si particles as compared to that in the initial *c*-Si target is noteworthy.

To assess the possibility of using the obtained ablated material in biomedical applications, we have measured the concentration of Si-NPs in as-formed suspensions (Table 2). Suspensions of mesopor-Si nanoparticles exhibit an increase in the particle concentration per unit volume, but the values do not exceed the maximum permissible concentration for biological experiments [2]. Therefore, the use of the proposed two-stage technology allows the quality of obtained Si-NP suspensions to be increased.

Table 1. Calculated laser ablation thresholds (J/cm^2) for *c*-Si and *por*-Si in water, ethanol, and air

Buffer medium	*c*-Si	Mesopor-Si	Micropor-Si
Water	1.26 ± 0.11	0.68 ± 0.05	0.18 ± 0.02
Ethanol	1.18 ± 0.09	0.63 ± 0.04	0.41 ± 0.04
Air	0.86 ± 0.09	1.21 ± 0.06	0.41 ± 0.02

Table 2. Concentration (mg/mL) of *c*-Si and *por*-Si nanoparticles obtained by laser ablation in water and ethanol

Buffer medium	*c*-Si	Mesopor-Si	Micropor-Si
Water	0.5	0.56	0.42
Ethanol	0.52	0.56	0.5

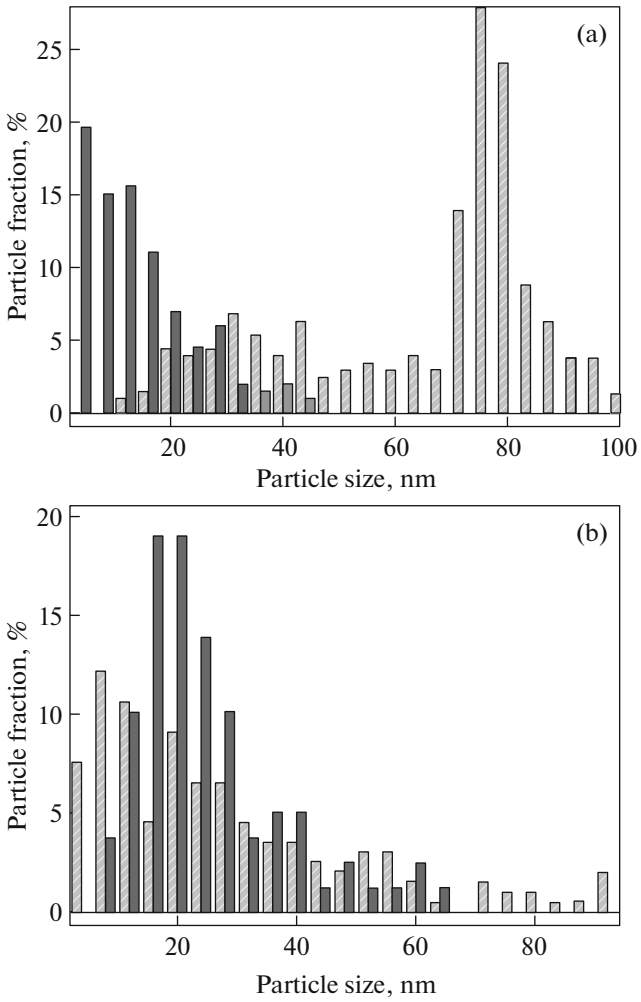

Fig. 2. Histograms of particle size distribution in laser-ablated micropor-Si (dark columns) and mesopor-Si (gray columns) suspensions in (a) distilled water and (b) ethanol.

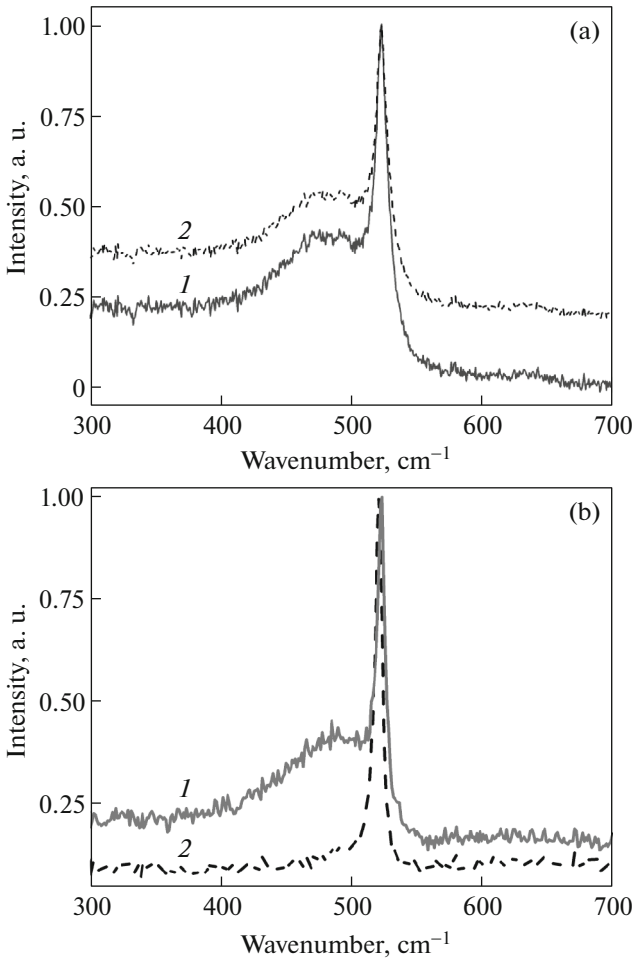

Fig. 3. Raman spectra of Si-NPs in suspensions obtained by laser ablation of (a) micropor-Si and (b) mesopor-Si targets in (*1*) distilled water and (*2*) ethanol.

The distribution of laser-ablated particles with respect to their dimensions was determined from the analysis of atomic-force microscopy (AFM) images obtained using an ND-MDT Solver-PRO scanning probe microscope. The obtained histograms were compared to SEM data. The comparative analysis of *por*-Si nanoparticle images obtained in the course of sequential electrochemical etching and picosecond pulsed laser ablation in distilled water and ethanol revealed the presence of a fraction of Si-NPs particles with dimensions below 20 nm (Fig. 2), which increases the possibilities and expands the prospects of their use for incorporation into biological tissues in comparison to mechanically comminuted *por*-Si. Note also that this fraction of Si-NPs obtained by ablation in ethanol is greater than that in the case of ablation in water (Fig. 2). This peculiarity is probably indicative of (i) lower efficiency of ablated material agglomeration into NPs in the ethanol buffer medium and (ii) formation of a fraction of relatively large particles (65–100 nm) during ablation in water due to Si-NPs coagulation into agglomerates. The presence of such a coarse agglomerated fraction was also confirmed by the SEM data. In addition, SEM images of the Si-NPs of all types showed that all these particles had a smooth, nearly spherical shape [12]. It is believed that this circumstance must favor the penetration of NPs into biological tissues at minimum mechanical damage.

The degree of crystallinity in laser-ablated Si-NPs was studied using their Raman spectra measured on a Horiba Jobin Yvon HR 800 spectrometer with Ar^+ laser excitation at a 488-nm wavelength. Figure 3 shows the Raman spectra of suspensions obtained by laser ablation of micropor-Si and mesopor-Si targets in distilled water and ethanol, which confirm the presence of a *c*-Si phase as displayed by the peak at 520 cm^{-1} and an amorphous phase manifested at 480–510 cm^{-1}. Note that the Raman spectra of suspensions obtained in water and ethanol are rather sim-

ilar. In the case of mesopor-Si ablation in water, the Raman spectrum of Si-NP suspension shows evidence of a greater amorphous fraction as compared to that in ethanol (Fig. 3).

In concluding, the obtained results showed that picosecond pulsed laser ablation of meso- and microporous silicon layers in water and ethanol can be used for the formation of nanosilicon suspensions with Si-NP diameters below 100 nm. It is established that the obtained nanoparticles possess a high degree of crystallinity and have reduced laser ablation threshold compared to that for *c*-Si, which favors using these Si-NPs for various applications in photonics and biomedicine.

ACKNOWLEDGEMENTS

This work was performed using instrumentation of the Teaching Methodological Center of Lithography and Microscopy at Moscow State University.

FUNDING

This work was supported by the Russian Science Foundation, project No. 18-32-00884_mol_a.

CONFLICT OF INTEREST

The authors declare that they have no conflict of interest.

REFERENCES

1. L. M. Bimbo, M. Sarparanta, H. A. Santos, A. J. Airaksinen, E. Mäkilä, T. Laaksonen, L. Peltonen, V.-P. Lehto, J. Hirvonen, and J. Salonen, ACS Nano **4**, 3023 (2010).
2. O. I. Ksenofontova, A. V. Vasin, V. V. Egorov, A. V. Bobyl', F. Yu. Soldatenkov, E. I. Terukov, V. P. Ulin, N. V. Ulin, and O. I. Kiselev, Tech. Phys. **59**, 66 (2014).
3. M. B. Gongalsky, L. A. Osminkina, A. Pereira, A. A. Manankov, A. A. Fedorenko, A. N. Vasiliev, V. V. Solovyev, A. A. Kudryavtsev, M. Sentis, and A. V. Kabashin, Sci. Rep. **6**, 24732 (2016).
4. S. V. Zabotnov, F. V. Kashaev, D. V. Shuleiko, M. B. Gongalsky, L. A. Golovan, P. K. Kashkarov, D. A. Loginova, P. D. Agrba, E. A. Sergeeva, and M. Yu. Kirillin, Quantum Electron. **47**, 638 (2017).
5. *Handbook of Porous Silicon*, Ed. by L. Canham (Springer, Cham, 2018).
6. E. Tolstik, L. A. Osminkina, C. Matthaus, M. Burkhardt, K. E. Tsurikov, U. A. Natashina, V. Y. Timoshenko, R. Heintzmann, J. Popp, and V. Sivakov, Nanomed.: Nanotechnol. Biol. Med. **12**, 1931 (2016).
7. V. Yu. Timoshenko, A. A. Kudryavtsev, L. A. Osminkina, A. S. Vorontsov, Yu. V. Ryabchikov, I. A. Belogorokhov, D. Kovalev, and P. K. Kashkarov, JETP Lett. **83**, 423 (2006).
8. A. V. Skobelkina, F. V. Kashaev, A. V. Kolchin, T. P. Kaminskaya, S. V. Zabotnov, L. A. Golovan', D. A. Loginova, A. V. Khilov, P. D. Agrba, and M. Yu. Kirillin, Uch. Zap. Fiz. Fak. MGU, No. 4, 1841302 (2018).
9. E. Yu. Loktionov, Yu. S. Protasov, and Yu. Yu. Protasov, Inzh. Zh.: Nauka Innov., No. 10 (2013). https://doi.org/10.18698/2308-6033-2013-10-1036
10. B. C. Stuart, M. D. Feit, S. Herman, A. M. Rubenchik, B. W. Shore, and M. D. Perry, Phys. Rev. B **53**, 1749 (1996).
11. W. Kautek, J. Krausz, M. Lenzner, S. Sartania, C. Spielmann, and F. Kraisz, Appl. Phys. Lett. **69**, 3146 (1996).
12. A. V. Skobelkina, F. V. Kashaev, S. V. Zabotnov, A. V. Kolchin, T. P. Kaminskaya, D. E. Presnov, E. A. Sergeeva, M. Yu. Kirillin, L. A. Golovan, and P. K. Kashkarov, in *Proceedings of the 4th International Conference on Nanotechnologies and Biomedical Engineering ICNBME 2019*, Ed. by I. Tiginyanu, V. Sontea, and S. Railean (Springer, Cham, 2019), p. 101.

Translated by P. Pozdeev